

# Symmetry-Aware Transformer-based Mirror Detection

Tianyu Huang<sup>1</sup>, Bowen Dong<sup>1</sup>, Jiaying Lin<sup>2</sup>, Xiaohui Liu<sup>1</sup>, Rynson W.H. Lau<sup>2</sup>,  
and Wangmeng Zuo<sup>1</sup>✉

<sup>1</sup>Harbin Institute of Technology <sup>2</sup>City University of Hong Kong

{tyhuang0428, cndongsky, lxh720199}@gmail.com,

jiayinlin5-c@my.cityu.edu.hk, rynson.lau@cityu.edu.hk, wmluo@hit.edu.cn

**Abstract.** Mirror detection aims to identify the mirror regions in the given input image. Existing works mainly focus on integrating the semantic features and structural features to mine the similarity and discontinuity between mirror and non-mirror regions, or introducing depth information to help analyze the existence of mirrors. In this work, we observe that a real object typically forms a loose symmetry relationship with its corresponding reflection in the mirror, which is beneficial in distinguishing mirrors from real objects. Based on this observation, we propose a dual-path Symmetry-Aware Transformer-based mirror detection Network (SATNet), which includes two novel modules: Symmetry-Aware Attention Module (SAAM) and Contrast and Fusion Decoder Module (CFDM). Specifically, we first introduce the transformer backbone to model global information aggregation in images, extracting multi-scale features in two paths. We then feed the high-level dual-path features to SAAMs to capture the symmetry relations. Finally, we fuse the dual-path features and refine our prediction maps progressively with CFDMs to obtain the final mirror mask. Experimental results show that SATNet outperforms both RGB and RGB-D mirror detection methods on all available mirror detection datasets. Codes and trained models are available at <https://github.com/tyhuang0428/SATNet>.

**Keywords:** Mirror Detection, Transformer, Symmetry

## 1 Introduction

Mirrors are common objects in the human world, and their presence can affect the performance of a range of vision tasks. For example, Zendel *et al.* [41] propose a list of potential hazards within the CV domain, and the existence of mirrors is one of them. However, mirrors can be challenging to detect by using some general detection methods from related tasks, such as salient object detection and semantic segmentation. As such, it is necessary to treat mirror detection as an independent vision task, and previous works [40, 16, 23] have managed to tackle this issue from either vision-only frameworks or RGB-D training paradigm.

Considering the reflection characteristics of mirrors, symmetry relationships between mirror and non-mirror regions are supposed to be an important cue for



**Fig. 1.** In (a), MirrorNet [40] and PMDNet [16] both dismiss the right half of the mirror. In (b), MirrorNet [40] takes right half of the image into consideration; PMDNet [16] count part of the similar non-mirror regions into mirrors. Modeling a loose symmetry relation we propose, our network SATNet succeeds in both cases. The loose symmetry relation can indicate the existence of mirrors (in case a) and suggest which side of the symmetry pair is a mirror (in case b).

mirror detection. In Fig. 1(a), the right half of the mirror would not be missed if the mirror detection model can detect the mirror symmetry relationship of the two paintings and identify which one should be in the mirror. In Fig. 1(b), if the model finds that the left power bank is the mirror image of another view of the right real power bank, it can then classify the right real power bank as a non-mirror region. [16,23] have already leveraged the similarity relationship, while the relationships sometimes come from the similarity among non-mirror regions. As shown in Fig. 1(b), if there is a large similar area in non-mirror regions, those methods can easily be misclassified as mirrors. In contrast to the ambiguous similarity relationship, we suggest mining a symmetry relationship caused by mirror reflection. We also notice that this symmetry relationship is highly dependent on the camera viewpoint. The paintings inside and outside mirrors form a nearly perfect reflection symmetry pair in Fig. 1(a), while the power banks inside and outside mirrors are from different views in Fig. 1(b). Even though real-world object and their reflection in mirrors may not be strictly symmetric regarding the position or orientation, they always maintain the semantic or luminance consistency with the same object. That is, an object in a mirror should be a mirror reflection of an object in the real world from a certain view. We regard this kind of relationship as loose symmetry and aim to explore a new solution to model and leverage this loose symmetry relationship for mirror detection.

Taking loose symmetry into account, we present our Symmetry-Aware Transformer based mirror detection Network (SATNet). In particular, we introduce a dual-path network to extract and enhance symmetric features, taking an input image as well as its corresponding horizontally flipped image as inputs. For modeling symmetry semantics, we propose a novel Symmetry-Aware Attention Module (SAAM) in high-level dual-path features. For mirror region segmentation, we propose a novel Contrast and Fusion Decoder Module (CFDM), constructing a pyramidal decoder, to fuse and refine the dual-path features progressively. Ad-

ditionally, since symmetric pairs are required to be analyzed in a global view, we employ a transformer-based model Swin Transformer [20] as our backbone to enlarge our receptive field.

Extensive experiments have been conducted to evaluate our proposed method. Our network SATNet outperforms the state-of-the-art methods on all the available mirror detection datasets. Albeit our SATNet does not use any depth information, it can even surpass the RGB-D method PDNet [23]. And our visualization results show that loose symmetry relationships are effective and beneficial for mirror detection.

To sum up, our main contributions include:

- We observe that there are typically loose symmetry relationships between mirror and non-mirror regions. Based on this observation, we propose a novel dual-path Symmetry-Aware Transformer-based mirror detection network (SATNet) to learn symmetry relations for mirror detection.
- We present a novel Symmetry-Aware Attention Module (SAAM) to extract high-level symmetry semantics and a novel Contrast and Fusion Decoder Module (CFDM) to refine multi-scale mirror features.
- Our network SATNet achieves state-of-the-art results on various mirror detection datasets. Experimental results clearly demonstrate the benefit of loose symmetry relationships for mirror detection.

## 2 Related Work

### 2.1 Mirror Detection

The mirror detection task aims to identify the mirror regions of the given input image. To tackle this problem, Yang *et al.* [40] proposed the first mirror detection network called MirrorNet, which focuses on modeling the contrasted features between the contexts inside and outside mirrors, but may fail when contrasts are too subtle to detect. Lin *et al.* [16] suggested a progressive mirror detection network (PMDNet). They designed a relational contextual contrasted local module to extract relational features, and an edge detection and fusion module to refine prediction with boundary detection. They also introduced similarity between mirror and non-mirror regions to this task, while we argue that similarity is too general and not specified for modeling the relationship between mirror and non-mirror regions. Recently, Mei *et al.* [23] introduced depth estimates to mirror detection. They proposed a dual-path mirror detection network PDNet, which integrates information from both image features and depth features. We find out that PDNet also has its limitations, as RGB-D methods can be misled by depth information, wrongly judging regions with significant depth changes as mirror boundaries. Different from existing works, we aim to utilize loose symmetry relationships between real-world objects and corresponding mirror regions to enhance the overall detection ability.

## 2.2 Reflection Symmetry Detection

Reflection symmetry detection aims to detect symmetry axes in given images. Early works in this task can be divided into two categories: keypoint matching detection and dense heatmap detection. For keypoint matching, Loy *et al.* [22] adopted SIFT [21] to compute matched keypoints, and generated potential symmetry axes accordingly. Cornelius *et al.* [6] took a single matching pair for hypothesizing with the local affine frame. For dense heatmap, Tsogkas *et al.* [34] utilized pixel-level features to densely predict the symmetry area. Funk *et al.* [15] employed CNNs to directly extract the symmetric features. Recently, Seo *et al.* [30] proposed a novel polar matching convolution to encode the similarities among pixels. Contrary to the strict reflection symmetry, symmetry relationships in mirror cases are loosely defined. Therefore, reflection symmetry detection methods cannot be directly employed in mirror detection. To tackle this, we propose a dual-path Transformer-based structure with attention mechanisms in high-level features to model the loose symmetry relationships.

## 2.3 Salient Object Detection

Salient object detection (SOD) aims to detect and segment the most distinct object in an input image. Existing methods in RGB SOD are mainly based on the UNet structure [29], like [37, 26].  $R^3$ Net [10] adopts a recurrent network to progressively refine the salient map. PiCANet [17] and PAGRNet [42] adopt attention mechanisms to learn more dependencies among features. Recently, RGB-D SOD has received considerable attention. Depth fusion methods are the key issue in this field. Several methods [32] treat depth as an additional dimension of the input features, while the others [12] separately extract RGB and depth features and fuse them in the decoding process. Liu *et al.* [18] proposed to fuse depth information with attention mechanisms. Pang *et al.* [25] integrated RGB and depth through densely connected structures. Liu *et al.* [19] proposed a vision transformer network, rethinking this field from an aspect of sequence-to-sequence architectures. Albeit similar to mirror detection, SOD methods can hardly have a good performance on the mirror detection task as mirrors are not salient enough to detect in most cases. SOD methods may wrongly detect some conspicuous objects inside mirrors.

## 3 Method

Based on the idea of loose symmetry relationships, we propose a dual-path Symmetry-Aware Transformer-based network for mirror detection. Loose symmetry relationships can assist the detecting process in two aspects: the presence of loose symmetry relationships implies the possible existence of mirrors; differences between symmetric pairs indicate which part belongs to the mirror regions. The dual-path structure and our novel Symmetry-Aware Attention Module are designed for the first aspect. Additionally, to better encode the symmetry features as well as recognize the corresponding mirror semantics, a transformer

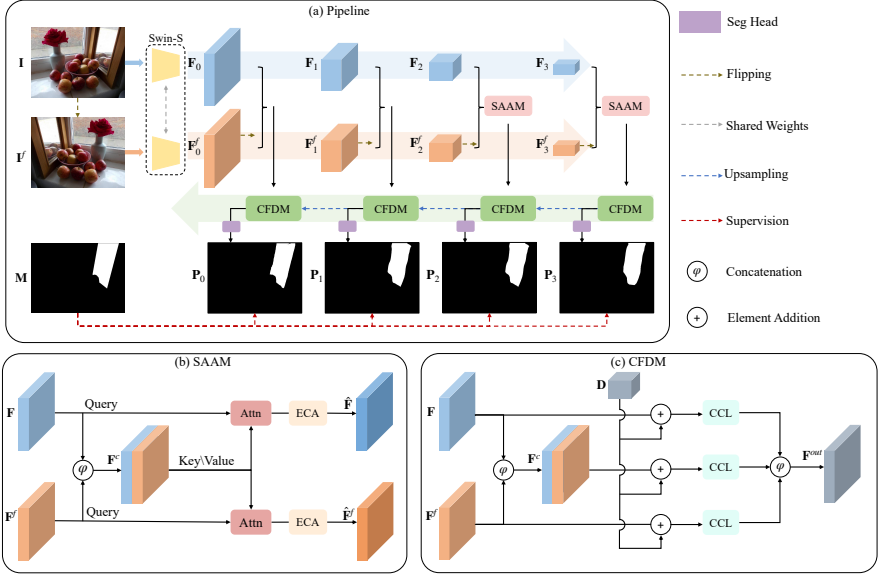


**Fig. 2.** (a) Pipeline of our SATNet. Firstly, the input image  $\mathbf{I}$  and the flipped image  $\mathbf{I}^f$  are fed into the same Swin transformer backbone to extract multi-scale features; Then, our Symmetry-Aware Attention Module (SAAM) is embedded to the highest two levels to learn symmetry semantics among the features and flipped features; Finally, our Contrast and Fusion Decoder Module (CFDM) fuse and refine previous multi-scale features by contrasts, and we get the final prediction map at the last decoder layer. (b) A Symmetry-Aware Attention Module (SAAM). (c) A Contrast and FusionDecoder Module (CFDM).

backbone and our Contrast and Fusion Decoder Module are proposed for the second aspect.

### 3.1 Overview

Fig. 2(a) illustrates the pipeline of our SATNet. Given an input image  $\mathbf{I}$  as well as its flipped image  $\mathbf{I}^f$ , we feed them into the same Swin transformer backbone to obtain multi-scale features  $\{\mathbf{F}_0, \dots, \mathbf{F}_3\}$  and corresponding flipped features  $\{\mathbf{F}_0^f, \dots, \mathbf{F}_3^f\}$ , respectively. For modeling symmetry relations, we select features from the highest two levels of both paths, and feed features in the same level into our Symmetry-Aware Attention Module (SAAM), fetching joint features  $\hat{\mathbf{F}}$  and  $\hat{\mathbf{F}}^f$ . Then, the multi-scale features  $\{\mathbf{F}_i / \hat{\mathbf{F}}_i\}$  as well as the flipped features  $\{\mathbf{F}_i^f / \hat{\mathbf{F}}_i^f\}$  are fed into corresponding Contrast and Fusion Decoder Module (CFDM), generating coarse output features  $\mathbf{F}_i^{out}$  with different scales progressively. For each  $\mathbf{F}_i^{out}$  (except  $\mathbf{F}_0^{out}$ ), we upsample it into the next decoder as the reference features  $\mathbf{D}_{i-1}$  for further prediction refinement. Meanwhile, we get the prediction map  $\mathbf{P}_i$  in each decoder through a segmentation head and supervise

it via the ground-truth mask  $\mathbf{M}$ . Finally, our prediction result  $\tilde{\mathbf{M}}$  is generated by the last decoder module for final evaluation.

### 3.2 Transformer for Mirror Detection

Loose symmetry is typically a long-range relationship, which means our network needs a large receptive field to perceive it. CNN-based methods utilize a couple of convolution kernels to fulfill local features aggregation. However, the convolution with small kernel size cannot construct global feature aggregation directly, which restricts the feature representation ability of those methods in complex scenarios. In contrast, the self-attention module in transformers can model the long-range interaction explicitly, making vision transformer very competitive in several complex scene understanding tasks [44]. Swin transformer [20] proposes regular and shifted window self-attention modules to construct local and global feature aggregation with limited computation complexity, while achieving state-of-the-art performance in scene parsing. Thus, we adopt Swin transformer as the backbone of our SATNet.

### 3.3 Dual-path Structure

In most cases, loose symmetry relationships are implicit under complex semantics. Such a relationship is too hidden to be perceived by existing baselines, which has been verified in our ablation study. To better perceive the relationship, dual enhancements are required. As a common method of data augmentation, horizontal flipping can modify the global semantics of natural images, while symmetry relationships still exist (they just display in an opposite direction). Thus, we introduce a dual-path network to extract symmetric features: Given  $\mathbf{F}$  and  $\mathbf{F}^f$  from both paths, we expect they differ from each other, but have features of the same loose symmetry relationship. When we concatenate them together as  $\mathbf{F}^c$ , symmetry semantics in the symmetric region can be enhanced. To extract the same symmetric features, input images  $\mathbf{I}$  and  $\mathbf{I}^f$  must be fed into the same backbone. Our fusion function is defined as follows:

$$\varphi(\mathbf{a}_1, \dots, \mathbf{a}_n) = \sigma(BN(\psi_{3 \times 3}(\psi_{1 \times 1}([\mathbf{a}_1, \dots, \mathbf{a}_n])))), \quad (1)$$

$$\mathbf{F}^c = \varphi(\mathbf{F}, \text{flip}(\mathbf{F}^f)), \quad (2)$$

where  $[\cdot, \dots, \cdot]$  denotes the concatenation operation on the channel dimension.  $\psi_{w \times w}$  is a  $w \times w$  convolution, BN denotes the Batch Normalization,  $\sigma$  is the ReLU activation function, and flip is the horizontal flipping. To align features in the spatial level during concatenation, we flip  $\mathbf{F}^f$  back before SAAM or CFDM.

### 3.4 Symmetry-Aware Attention Module

Fig. 2(b) shows the architecture of our symmetry-aware attention module (SAAM). With SAAM, we aim to perceive loose symmetry relationships in an image that

indicates the possible existence of mirrors. To this end, we use the attention mechanisms (i) to enhance the feature  $\mathbf{F}$  of the input image as well as (ii) to obtain the symmetry-aware feature by modeling the dependency between the input and its flipped images. In general, the attention mechanism can model the dependencies among each position in a global manner [35], which can be formulated as,

$$\text{Attention}(\mathbf{Q}, \mathbf{K}, \mathbf{V}) = \text{Softmax}\left(\frac{\mathbf{Q}\mathbf{K}^T}{\sqrt{d_k}}\right)\mathbf{V}, \quad (3)$$

where  $\mathbf{Q}$ ,  $\mathbf{K}$  and  $\mathbf{V}$  denote Query, Key and Value, respectively.

Our SAAM takes both  $\mathbf{F}^c$  as well as  $\mathbf{F}$  and  $\mathbf{F}^f$  as the input. Among them,  $\mathbf{F}^c$  aggregates the features from  $\mathbf{F}$  and  $\mathbf{F}^f$  from both paths, and is spatially consistent with  $\mathbf{F}$ , and thus can be treated as an augmented representation of  $\mathbf{F}$ . To exploit the attention to enhance the feature  $\mathbf{F}$ , we treat  $\mathbf{F}$  as query and  $\mathbf{F}^c$  as key and value, and further apply channel transformation with Efficient Channel Attention (ECA) [36] module right after the attention module to obtain the enhanced feature  $\hat{\mathbf{F}}$ ,

$$\hat{\mathbf{F}} = \text{ECA}(\text{Attention}(\mathbf{F}, \mathbf{F}^c, \mathbf{F}^c)), \quad (4)$$

where  $\text{ECA}(\cdot)$  denotes the Efficient Channel Attention module. To obtain the symmetry-aware feature, we treat  $\mathbf{F}^f$  as query and  $\mathbf{F}^c$  as key and value. Note that  $\mathbf{F}^f$  is extracted from the flipped image and  $\mathbf{F}^c$  is spatially consistent with the input image. Their similarity score can thus be treated as an indicator of loose mirror symmetry between parts from the input and its flipped images. And the output of the attention module can then be regarded to be symmetry-aware. Analogous to  $\hat{\mathbf{F}}$ , the symmetry-aware feature is obtained by,

$$\hat{\mathbf{F}}^f = \text{ECA}(\text{Attention}(\mathbf{F}^f, \mathbf{F}^c, \mathbf{F}^c)). \quad (5)$$

### 3.5 Contrast and Fusion Decoder Module

Fig. 2(c) shows the Contrast and Fusion Decoder Module (CFDM) for fusing the two paths of features and refining our prediction maps. Since MirrorNet [40], Context Contrast Local (CCL) decoder [11] has been widely adopted as a module in mirror detection networks [40,16,23]. In this subsection, we further extend the CCL decoder to present our CFDM for handling multiple features. As shown in Fig. 2, our CFDM takes  $\mathbf{F}_i$  and  $\mathbf{F}_i^f$  as the input when  $i = 0, 1$ , and  $\hat{\mathbf{F}}_i$  and  $\hat{\mathbf{F}}_i^f$  when  $i = 2, 3$ . Without loss of generality, we use  $\mathbf{F}_i$  and  $\mathbf{F}_i^f$  as an example to explain the CFDM module.

To begin with, we use Eq. (2) to obtain the fused feature  $\mathbf{F}_i^c$ . Denote by  $\mathbf{F}_{i+1}^{\text{out}}$  the  $(i+1)$ -scale CFDM output. We then upsample  $\mathbf{F}_{i+1}^{\text{out}}$  to obtain the higher-level feature map,

$$\mathbf{D}_i = U_2(\sigma(BN(\psi_{3 \times 3}(\mathbf{F}_{i+1}^{\text{out}}))), \quad (6)$$

where  $U_2$  denotes the bilinear upsampling operation. Subsequently, the reference features for  $(\mathbf{F}_i^c, \mathbf{F}_i, \mathbf{F}_i^f)$  can be given by,

$$(\tilde{\mathbf{F}}_i^c, \tilde{\mathbf{F}}_i, \tilde{\mathbf{F}}_i^f) = \begin{cases} (\mathbf{F}_i^c, \mathbf{F}_i, \mathbf{F}_i^f) \oplus (\mathbf{D}_i, \mathbf{D}_i, \mathbf{D}_i), & i < 3 \\ (\mathbf{F}_i^c, \mathbf{F}_i, \mathbf{F}_i^f), & i = 3 \end{cases} \quad (7)$$

where  $\oplus$  denotes the element-wise summation operator.

The three feature maps  $\tilde{\mathbf{F}}_i^c, \tilde{\mathbf{F}}_i, \tilde{\mathbf{F}}_i^f$  are separately fed into the CCL module to extract contrastive semantics. Here we use  $\tilde{\mathbf{F}}_i$  as an example,

$$CCL(\tilde{\mathbf{F}}_i) = \sigma(BN(f_l(\tilde{\mathbf{F}}_i) - f_{ct}(\tilde{\mathbf{F}}_i))), \quad (8)$$

where  $f_l$  is the local feature extractor which contains a  $3 \times 3$  convolution with a dilation rate of 1, BN, and ReLU in turn.  $f_{ct}$  is the content feature extractor which is similar to  $f_l$  but with different dilation rates [11]. Considering the changes on the receptive field, we set dilation rates to  $\{8, 6, 4, 2\}$  for layer  $\{0, 1, 2, 3\}$ , respectively. Finally, we concatenate those three CCL outputs together to get the output features  $\mathbf{F}_i^{out}$  and the corresponding prediction map  $\mathbf{P}_i$ , which is given as follows,

$$\mathbf{F}_i^{out} = \varphi(CCL(\tilde{\mathbf{F}}_i^c), CCL(\tilde{\mathbf{F}}_i), CCL(\tilde{\mathbf{F}}_i^f)), \quad (9)$$

$$\mathbf{P}_i = f_{seg}(\mathbf{F}_i^{out}), \quad (10)$$

where  $f_{seg}$  is a segmentation head whose output has 2 channels. And the output of the last decoder layer  $\mathbf{P}_0$  is adopted as the final prediction result  $\tilde{\mathbf{M}}$  of our network.

### 3.6 Loss Function

Our learning objective is defined by considering all scales. For each prediction map  $\mathbf{P}_i$ , we calculate the binary cross-entropy (BCE) loss [8] between  $\mathbf{P}_i$  and the ground-truth  $\mathbf{M}$ . The overall loss function  $\mathcal{L}$  is then given as the summation of BCE loss for each prediction map,

$$\mathcal{L} = \sum_{i=0}^3 w_i \mathcal{L}_{bce}(\mathbf{P}_i, \mathbf{M}), \quad (11)$$

where  $w_i$  is the corresponding weight for the  $i$ -th layer. We empirically set the weight  $w_i$  as  $[1.25, 1.25, 1.0, 1.5]$  according to the experimental results.

## 4 Experiments

### 4.1 Datasets

Following previous works [40, 16], we use Mirror Segmentation Dataset (MSD) and Progressive Mirror Dataset (PMD) to evaluate our method. Besides, we

also adopt an RGB-D dataset RGBD-Mirror to make a comparison with the state-of-the-art RGB-D mirror detection method PDNet [23]. MSD is the first proposed mirror detection dataset with 3,063 images for training and 955 images for testing. All of the images are captured by Yang *et al.* [40] themselves and manually annotated. PMD is collected from six public datasets: ADE20K [45,46], NYUD-V2 [31], MINC [3], Pascal-Context [24], SUNRGBD [33], and COCO-Stuff [4]. It has 5,095 images for training and 571 images for testing, and is more challenging than MSD. RGBD-Mirror is the first mirror dataset with depth information. It is composed from four popular RGB-D datasets: Matterport3D [5], SUN- RGBD [33], ScanNet [7] and 2D3DS [2], with 2,000 images for training and 1,049 images for testing.

## 4.2 Evaluation Metrics

Following previous works [40,16], we adopt three commonly used dense prediction evaluation metrics: intersection over union (IoU), F-measure  $F_\beta$ , and mean absolute error (MAE) to assess mirror detection performance.

**IoU** is computed by the intersection and union of the ground-truth and prediction map:

$$IoU = \frac{\mathbf{M} \cap \tilde{\mathbf{M}}}{\mathbf{M} \cup \tilde{\mathbf{M}}}, \quad (12)$$

**F-measure** is computed by the precision and recall of the prediction result:

$$F_\beta = \frac{(1 + \beta^2) \times Precision \times Recall}{\beta^2 \times Precision + Recall}, \quad (13)$$

where  $\beta^2$  is set as 0.3, which is suggested by [1].

**MAE** is the rate of mean absolute error:

$$MAE = \frac{1}{W \times H} \sum_{i=1}^W \sum_{j=1}^H |\tilde{\mathbf{M}}(i, j) - \mathbf{M}(i, j)|, \quad (14)$$

where  $W$  and  $H$  are width and height of the image.

## 4.3 Implementation Details

We implement our network on PyTorch [28] and use the small version of Swin Transformer (namely Swin-S) pretrained on ImageNet-1k [9] as the backbone of our network. Note that dual-path features are fed into the same backbone and share the weights. Following data augmentation methods adopted by previous works, we adopt random resize and crop as well as random horizontal flipping to augment training images. And for testing, we simply resize input images to  $512 \times 512$  to evaluate our network. Our network is trained on 8 Tesla V100 GPUs with 2 images per GPU for 20K iterations. During training, we use ADAM weight decay optimizer (AdamW) and set  $\beta_1$ ,  $\beta_2$ , and the weight decay to 0.9, 0.999, and 0.01, respectively. The learning rate is initialized to  $6 \times 10^{-4}$  and decayed by the *poly* strategy with the power of 1.0. It takes 6 hours to train our network. and testing on a single GPU needs 0.08s per image.

**Table 1.** Quantitative results of the state-of-the-art methods on MSD dataset and PMD dataset. The best results are shown in bold. Our method achieves the best performance in terms of all the evaluation metrics.

Method	Pub. Year	MSD			PMD		
		$IoU \uparrow$	$F_\beta \uparrow$	$MAE \downarrow$	$IoU \uparrow$	$F_\beta \uparrow$	$MAE \downarrow$
CPDNet [39]	CVPR'19	57.58	0.743	0.115	60.04	0.733	0.041
MINet [27]	CVPR'20	66.39	0.823	0.087	60.83	0.798	0.037
LDF [38]	CVPR'20	72.88	0.843	0.068	63.31	0.796	0.037
VST [19]	ICCV'21	79.09	0.867	0.052	59.06	0.769	0.035
SETR [44]	CVPR'21	68.97	0.851	0.071	57.44	0.797	0.034
MirrorNet [40]	ICCV'19	78.88	0.856	0.066	58.51	0.741	0.043
PMDNet [16]	CVPR'20	81.54	0.892	0.047	66.05	0.792	0.032
SATNet(Ours)	-	<b>85.16</b>	<b>0.923</b>	<b>0.033</b>	<b>69.24</b>	<b>0.847</b>	<b>0.024</b>

**Table 2.** Quantitative results of the state-of-the-art methods on RGBD-Mirror dataset. w/ Depth denotes the usage of depth information in a corresponding method. Our method outperforms all the competing methods, even though we do not use depth information.

Method	Pub. Year	w/ Depth	RGBD-Mirror		
			$IoU \uparrow$	$F_\beta \uparrow$	$MAE \downarrow$
HDFNet [25]	ECCV'20	✓	44.73	0.733	0.093
S2MA [18]	CVPR'20	✓	60.87	0.781	0.070
JL-DCF [14]	CVPR'20	✓	69.65	0.844	0.056
DANet [43]	ECCV'20	✓	67.81	0.835	0.060
BBSNet [13]	ECCV'20	✓	74.33	0.868	0.046
VST [19]	ICCV'21	✓	70.20	0.851	0.052
PDNet [23]	CVPR'21	✗	73.57	-	0.053
PDNet [23]	CVPR'21	✓	77.77	0.878	0.041
SATNet(Ours)	-	✗	<b>78.62</b>	<b>0.905</b>	<b>0.031</b>

#### 4.4 Comparison with State-of-the-arts

To assess SATNet, we extensively compare it with several state-of-the-art methods. As shown in Table 1, we select 7 state-of-the-art methods for the comparison on MSD dataset and PMD dataset, including 4 RGB salient object detection methods CPDNet [39], MINet [27], LDF [38], and VST [19], 1 semantic segmentation method SETR [44], and 2 mirror detection methods MirrorNet [40] and PMDNet [16]. Our network outperforms other methods in terms of all the evaluation metrics. Fig. 3 provides the visualized comparison with those methods. The first three rows are examples of loose symmetry relationships. Our network can precisely distinguish real-world objects from their mirror reflections. In the first row, the cartoon toy and its reflection in mirrors cannot construct an obvious reflection symmetry, but our network can still perceive which part is in mirrors. Albeit PMDNet [16] has a specific module for modeling similarity relationship, it fails in handling an easy case in the third row, in which a chalk eraser is reflected in the mirror. The last two rows have scenes where mirrors are sim-

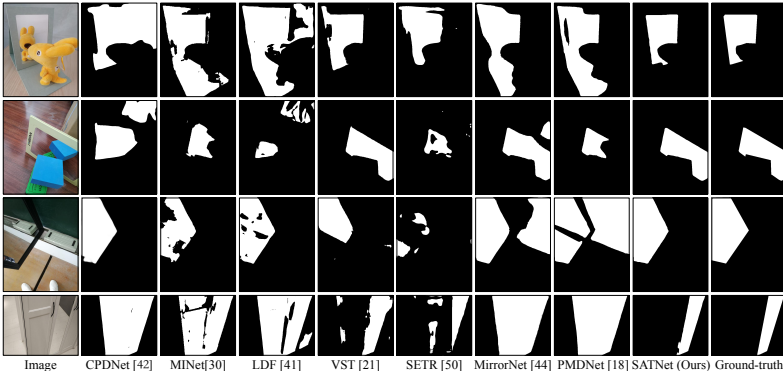


**Fig. 3.** Visualization results on MSD and PMD datasets. The first three rows are examples of loose symmetry relationships. The last row has scenes where mirrors are similar to their surroundings.

ilar to their surroundings. Our method can well exclude the non-mirror region, while the competing methods tend to classify the similar area as mirror region, especially the two mirror detection methods, which treat the whole similar area as the mirror region. The results show that symmetry-awareness is beneficial for mirror detection, and our method can utilize the symmetry information well.

Our method is also compared with six RGB-D salient object detection methods HDFNet [25], S2MA [18], JL-DCF [14], DANet [43], BBSNet [13], VST [19], and a mirror detection method PDNet [23] on the RGBD-Mirror dataset. As shown in Table 2, our method does not leverage depth information, and can still achieve the best performance in terms of all the evaluation metrics. Visualization results are shown in Fig. 4. We do not display HDFNet [25] for its poor quantitative performance in mirror detection. In all the five examples, RGB-D methods are likely to be misled by depth information. In the first two rows, they wrongly judge the depth changes as the existence of mirrors. In the third row, RGB-D methods can hardly detect symmetry relations. In comparison, our method correctly detects the mirror region by exploiting the loose symmetry relationship between the television and its reflection, while some competing methods even fail to detect the correct side of the mirror. In the fourth row, there is a mirror that can be easily missed. All the competing methods ignore the left mirror, although the depth map has an obvious change in that area. Our method can still discover the mirror as the scene in it have a kind of symmetry relation with the nearby cabinet. In the last row, we note that our method does not mis-detect the glasses region as a mirror region, while the competing methods can hardly tell the subtle differences between mirrors and glasses. Different from mirrors, glasses can transmit most of the lights, which weakens the reflection effects. It shows that our method can identify corresponding reflection features from mirrors. All the cases show that utilizing symmetry information can greatly benefit the performance of mirror detection, especially in complex scenes.

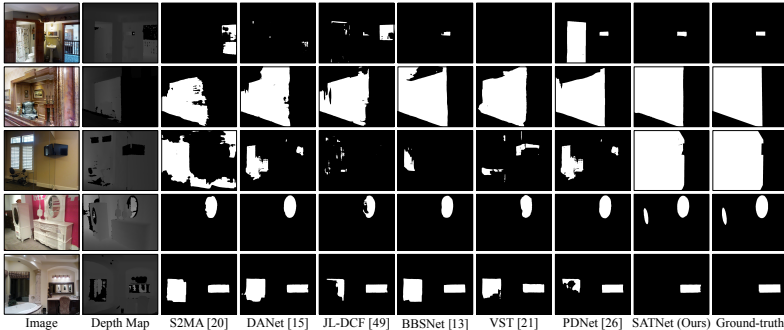


**Fig. 4.** Visualization results on RGB-D dataset. While our network does not utilize depth information, it is comparable or better than the state-of-the-art RGB-D methods. In the first two rows, changes in depth can easily affect the judgement of RGB-D methods. The third row contains a pair of symmetric objects inside and outside mirrors. The fourth row represents mirrors that can hardly be recognized. And the last row is a scene including both glasses and mirrors.

**Table 3.** Ablation study results on MSD. Swin-S is our baseline method which is decoded by UperNet. Dual-Path denotes the dual-path Swin Transformer. SAAM denotes our Symmetry-Aware Attention Module on scale 3. SAAMs denotes SAAM on both scale 2 and scale 3. CFDM denotes our Contrast and Fusion Decoder Module.

Method	$IoU \uparrow$	$F_\beta \uparrow$	$MAE \downarrow$
Baseline	80.46	0.901	0.045
Dual-Path	79.59	0.903	0.044
Dual-Path + SAAM	80.01	0.918	0.042
Dual-Path + SAAMs	80.03	0.903	0.043
Dual-Path + CFDM	81.98	0.918	0.039
Dual-Path + SAAM + CFDM	82.96	0.911	0.039
SATNet(Ours)	<b>85.16</b>	<b>0.923</b>	<b>0.033</b>

#### 4.5 Ablation study

**Benefits of Dual-Path Structure.** To better analyze the benefits of our dual-path structure, we conduct two experiments: One is a pure Swin Transformer decoded by UperNet (1st row); the other is a dual-path Swin Transformer, where features are trained and supervised separately in two paths (2nd row). Results in the first two rows show that, with extra features and supervision, the second method has no clear advantage when compared against the first one. That is to say, we cannot simply attribute the improvement of our method to the extra features we extract. Albeit we introduce the dual-path structure to enhance the symmetry semantics, the extra features are more like a repeated computation of the original ones if there are no appropriate fusing and matching mechanisms for the two paths.

**Effect of SAAM.** To evaluate the effect of our attention module, we conduct another two experiments: One is a dual-path Swin Transformer with a SAAM in the highest level (3-rd row), and the other is the same structure, but with SAAMs in the highest two levels (4-th row). Comparing the third row with the second row, we discover that “Dual-Path + SAAM” get better results in all the three metrics, especially 1.5% in  $F_\beta$ . The result is reasonable as our SAAM models symmetry relationship in high-level features. However,  $F_\beta$  in the fourth row drops back to 0.903, indicating that directly applying SAAM to features in lower levels may not work well. We further visualize the attention map in SAAM. In Fig. 5(c), the mirror region (green contour in (b)) of the attention map focuses on the mirror itself. In Fig. 5(d), the power bank region inside the mirror (red contour in (b)) in the attention map focuses on the power bank outside the mirror, and the highest attention signal is located on the real power bank in the image. This observation supports that SAAM is able to model loose symmetry relations.

**Effect of CFDM.** In the fifth row, we conduct an experiment based on the second row, replacing the UperNet decoder with our CFDM. Comparing results of the two rows, ”Dual-Path + CFDM” have a gain of 2.39%, 1.50%, and 0.5% in  $IoU$ ,  $F_\beta$ , and  $MAE$ , respectively. The improvement proves that our decoder module can properly fuse features in two paths and is more suitable for the mirror detection task.

**Combination of SAAM and CFDM.** To explore the best way to combine our SAAM and CFDM, we conduct two experiments: one is a dual-path Swin Transformer with a SAAM in the highest level and CFDMs as the decoder (6th row), and the other is our final network SATNet, which has SAAMs in the highest two levels (last row). Analyzing the last three rows, we conclude that applying SAAM before CFDM is effective as the three evaluation metrics have progressively improved to 85.16%, 0.923 and 0.033. On the other hand, comparing the network in the fourth row with SATNet, the improvement from “Dual-Path + SAAMs” to SATNet is even larger, which means our CFDM contributes to the fusion of dual-path features, especially in the high level.

**Visualization results for the ablation study.** To further analyze the effectiveness of each component, we visualize the prediction results of Swin-S, Dual-Path + SAAM, Dual-Path + CFDM, and our network SATNet in Fig. 6. Swin-S can provide the approximate location of the mirror, but is not sensitive to symmetry relationship, which demonstrates that current baselines can hardly model loose symmetry relationships. Equipped with our attention module SAAM, the network can exclude the real-world object which shades the mirror from the mirror region, showing the ability of perceiving symmetry relationships. However, its prediction map is not precise enough, especially near the boundary of mirrors. In comparison to our SAAM, our decoder module CFDM refines the mirror

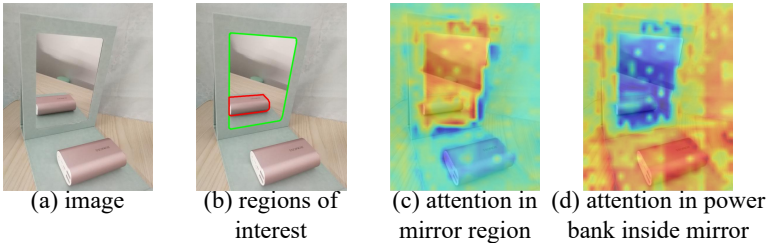


**Fig. 5.** Visualization of the attention maps in SAAM.

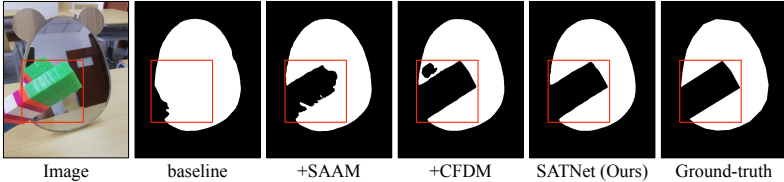


**Fig. 6.** Visualization results for the ablation study. In this example, our baseline Swin-S cannot perceive the symmetry relationship. The network embedded with SAAM does not outline a precise boundary. And when adding CFDM, the network is still confused about the symmetry relationship. Only SATNet can correctly detect the mirror region.

boundary well, but it wrongly excludes the symmetry area in the mirror region. Analogous to Swin-S, it cannot handle symmetry relationships well. Only with both two modules, our final network SATNet marks the mirror region correctly. The visualization result is basically consistent with the corresponding effects of the components we expect.

## 5 Conclusion

In this paper, we proposed a dual-path Symmetry-Aware Transformer-based mirror detection network (SATNet) for better mirror detection. We presented a new perspective to detect mirrors by leveraging loose symmetry relationships. Then, we suggested a dual-path network, introducing Swin Transformer as the backbone to enhance the ability of long-range dependencies understanding. Furthermore, we proposed the Symmetry-Aware Attention Module (SAAM) to aggregate better feature representation of symmetry relations, while exploiting Contrast and Fusion Decoder Module (CFDM) to generate refined prediction maps progressively. Experimental results on multiple datasets demonstrate the benefit of loose symmetry relationships in mirror detection. Our network can effectively model such relationships and greatly improve the performance of mirror detection in comparison to state-of-the-arts.

## References

1. Achanta, R., Hemami, S., Estrada, F., Susstrunk, S.: Frequency-tuned salient region detection. In: 2009 IEEE conference on computer vision and pattern recognition. pp. 1597–1604. IEEE (2009)
2. Armeni, I., Sax, S., Zamir, A.R., Savarese, S.: Joint 2d-3d-semantic data for indoor scene understanding. arXiv preprint arXiv:1702.01105 (2017)
3. Bell, S., Upchurch, P., Snavely, N., Bala, K.: Material recognition in the wild with the materials in context database. In: Proceedings of the IEEE conference on computer vision and pattern recognition. pp. 3479–3487 (2015)
4. Caesar, H., Uijlings, J., Ferrari, V.: Coco-stuff: Thing and stuff classes in context. In: Proceedings of the IEEE conference on computer vision and pattern recognition. pp. 1209–1218 (2018)
5. Chang, A., Dai, A., Funkhouser, T., Halber, M., Niessner, M., Savva, M., Song, S., Zeng, A., Zhang, Y.: Matterport3d: Learning from rgb-d data in indoor environments. arXiv preprint arXiv:1709.06158 (2017)
6. Cornelius, H., Loy, G.: Detecting bilateral symmetry in perspective. In: 2006 Conference on Computer Vision and Pattern Recognition Workshop (CVPRW'06). pp. 191–191. IEEE (2006)
7. Dai, A., Chang, A.X., Savva, M., Halber, M., Funkhouser, T., Nießner, M.: Scannet: Richly-annotated 3d reconstructions of indoor scenes. In: Proceedings of the IEEE conference on computer vision and pattern recognition. pp. 5828–5839 (2017)
8. De Boer, P.T., Kroese, D.P., Mannor, S., Rubinstein, R.Y.: A tutorial on the cross-entropy method. Annals of operations research **134**(1), 19–67 (2005)
9. Deng, J., Dong, W., Socher, R., Li, L.J., Li, K., Fei-Fei, L.: Imagenet: A large-scale hierarchical image database. In: 2009 IEEE conference on computer vision and pattern recognition. pp. 248–255. Ieee (2009)
10. Deng, Z., Hu, X., Zhu, L., Xu, X., Qin, J., Han, G., Heng, P.A.: R3net: Recurrent residual refinement network for saliency detection. In: Proceedings of the 27th International Joint Conference on Artificial Intelligence. pp. 684–690. AAAI Press (2018)
11. Ding, H., Jiang, X., Shuai, B., Liu, A.Q., Wang, G.: Context contrasted feature and gated multi-scale aggregation for scene segmentation. In: Proceedings of the IEEE Conference on Computer Vision and Pattern Recognition (CVPR) (June 2018)
12. Fan, D.P., Lin, Z., Zhang, Z., Zhu, M., Cheng, M.M.: Rethinking rgb-d salient object detection: Models, data sets, and large-scale benchmarks. IEEE Transactions on neural networks and learning systems **32**(5), 2075–2089 (2020)
13. Fan, D.P., Zhai, Y., Borji, A., Yang, J., Shao, L.: Bbs-net: Rgb-d salient object detection with a bifurcated backbone strategy network. In: European Conference on Computer Vision. pp. 275–292. Springer (2020)
14. Fu, K., Fan, D.P., Ji, G.P., Zhao, Q.: Jl-dcf: Joint learning and densely-cooperative fusion framework for rgb-d salient object detection. In: Proceedings of the IEEE/CVF Conference on Computer Vision and Pattern Recognition (CVPR) (June 2020)
15. Funk, C., Liu, Y.: Beyond planar symmetry: Modeling human perception of reflection and rotation symmetries in the wild. In: Proceedings of the IEEE international conference on computer vision. pp. 793–803 (2017)
16. Lin, J., Wang, G., Lau, R.W.: Progressive mirror detection. In: Proceedings of the IEEE/CVF Conference on Computer Vision and Pattern Recognition. pp. 3697–3705 (2020)

17. Liu, N., Han, J., Yang, M.H.: Picanet: Learning pixel-wise contextual attention for saliency detection. In: Proceedings of the IEEE Conference on Computer Vision and Pattern Recognition (CVPR) (June 2018)
18. Liu, N., Zhang, N., Han, J.: Learning selective self-mutual attention for rgb-d saliency detection. In: Proceedings of the IEEE/CVF Conference on Computer Vision and Pattern Recognition (CVPR) (June 2020)
19. Liu, N., Zhang, N., Wan, K., Shao, L., Han, J.: Visual saliency transformer. In: Proceedings of the IEEE/CVF International Conference on Computer Vision (ICCV). pp. 4722–4732 (October 2021)
20. Liu, Z., Lin, Y., Cao, Y., Hu, H., Wei, Y., Zhang, Z., Lin, S., Guo, B.: Swin transformer: Hierarchical vision transformer using shifted windows. arXiv preprint arXiv:2103.14030 (2021)
21. Lowe, D.G.: Distinctive image features from scale-invariant keypoints. International journal of computer vision **60**(2), 91–110 (2004)
22. Loy, G., Eklundh, J.O.: Detecting symmetry and symmetric constellations of features. In: European Conference on Computer Vision. pp. 508–521. Springer (2006)
23. Mei, H., Dong, B., Dong, W., Peers, P., Yang, X., Zhang, Q., Wei, X.: Depth-aware mirror segmentation. In: Proceedings of the IEEE/CVF Conference on Computer Vision and Pattern Recognition. pp. 3044–3053 (2021)
24. Mottaghi, R., Chen, X., Liu, X., Cho, N.G., Lee, S.W., Fidler, S., Urtasun, R., Yuille, A.: The role of context for object detection and semantic segmentation in the wild. In: Proceedings of the IEEE conference on computer vision and pattern recognition. pp. 891–898 (2014)
25. Pang, Y., Zhang, L., Zhao, X., Lu, H.: Hierarchical dynamic filtering network for rgb-d salient object detection. In: Computer Vision–ECCV 2020: 16th European Conference, Glasgow, UK, August 23–28, 2020, Proceedings, Part XXV 16. pp. 235–252. Springer (2020)
26. Pang, Y., Zhao, X., Zhang, L., Lu, H.: Multi-scale interactive network for salient object detection. In: Proceedings of the IEEE/CVF Conference on Computer Vision and Pattern Recognition (CVPR) (June 2020)
27. Pang, Y., Zhao, X., Zhang, L., Lu, H.: Multi-scale interactive network for salient object detection. In: Proceedings of the IEEE/CVF Conference on Computer Vision and Pattern Recognition. pp. 9413–9422 (2020)
28. Paszke, A., Gross, S., Massa, F., Lerer, A., Bradbury, J., Chanan, G., Killeen, T., Lin, Z., Gimelshein, N., Antiga, L., et al.: Pytorch: An imperative style, high-performance deep learning library. Advances in neural information processing systems **32**, 8026–8037 (2019)
29. Ronneberger, O., Fischer, P., Brox, T.: U-net: Convolutional networks for biomedical image segmentation. In: International Conference on Medical image computing and computer-assisted intervention. pp. 234–241. Springer (2015)
30. Seo, A., Shim, W., Cho, M.: Learning to discover reflection symmetry via polar matching convolution. In: Proceedings of the IEEE/CVF International Conference on Computer Vision (ICCV). pp. 1285–1294 (October 2021)
31. Silberman, N., Hoiem, D., Kohli, P., Fergus, R.: Indoor segmentation and support inference from rgbd images. In: European conference on computer vision. pp. 746–760. Springer (2012)
32. Song, H., Liu, Z., Du, H., Sun, G., Le Meur, O., Ren, T.: Depth-aware salient object detection and segmentation via multiscale discriminative saliency fusion and bootstrap learning. IEEE Transactions on Image Processing **26**(9), 4204–4216 (2017)

33. Song, S., Lichtenberg, S.P., Xiao, J.: Sun rgb-d: A rgb-d scene understanding benchmark suite. In: Proceedings of the IEEE conference on computer vision and pattern recognition. pp. 567–576 (2015)
34. Tsogkas, S., Kokkinos, I.: Learning-based symmetry detection in natural images. In: European Conference on Computer Vision. pp. 41–54. Springer (2012)
35. Vaswani, A., Shazeer, N., Parmar, N., Uszkoreit, J., Jones, L., Gomez, A.N., Kaiser, L., Polosukhin, I.: Attention is all you need. In: Advances in neural information processing systems. pp. 5998–6008 (2017)
36. Wang, Q., Wu, B., Zhu, P., Li, P., Zuo, W., Hu, Q.: Eca-net: Efficient channel attention for deep convolutional neural networks. In: IEEE/CVF Conference on Computer Vision and Pattern Recognition (CVPR) (June 2020)
37. Wang, T., Borji, A., Zhang, L., Zhang, P., Lu, H.: A stagewise refinement model for detecting salient objects in images. In: Proceedings of the IEEE International Conference on Computer Vision (ICCV) (Oct 2017)
38. Wei, J., Wang, S., Wu, Z., Su, C., Huang, Q., Tian, Q.: Label decoupling framework for salient object detection. In: Proceedings of the IEEE/CVF Conference on Computer Vision and Pattern Recognition (CVPR) (June 2020)
39. Wu, Z., Su, L., Huang, Q.: Cascaded partial decoder for fast and accurate salient object detection. In: Proceedings of the IEEE/CVF Conference on Computer Vision and Pattern Recognition. pp. 3907–3916 (2019)
40. Yang, X., Mei, H., Xu, K., Wei, X., Yin, B., Lau, R.W.: Where is my mirror? In: Proceedings of the IEEE/CVF International Conference on Computer Vision. pp. 8809–8818 (2019)
41. Zendel, O., Honauer, K., Murschitz, M., Humenberger, M., Fernandez Dominguez, G.: Analyzing computer vision data—the good, the bad and the ugly. In: Proceedings of the IEEE Conference on Computer Vision and Pattern Recognition. pp. 1980–1990 (2017)
42. Zhang, X., Wang, T., Qi, J., Lu, H., Wang, G.: Progressive attention guided recurrent network for salient object detection. In: Proceedings of the IEEE Conference on Computer Vision and Pattern Recognition. pp. 714–722 (2018)
43. Zhao, X., Zhang, L., Pang, Y., Lu, H., Zhang, L.: A single stream network for robust and real-time rgb-d salient object detection. In: European Conference on Computer Vision. pp. 646–662. Springer (2020)
44. Zheng, S., Lu, J., Zhao, H., Zhu, X., Luo, Z., Wang, Y., Fu, Y., Feng, J., Xiang, T., Torr, P.H., Zhang, L.: Rethinking semantic segmentation from a sequence-to-sequence perspective with transformers. In: Proceedings of the IEEE/CVF Conference on Computer Vision and Pattern Recognition (CVPR). pp. 6881–6890 (June 2021)
45. Zhou, B., Zhao, H., Puig, X., Fidler, S., Barriuso, A., Torralba, A.: Scene parsing through ade20k dataset. In: Proceedings of the IEEE conference on computer vision and pattern recognition. pp. 633–641 (2017)
46. Zhou, B., Zhao, H., Puig, X., Xiao, T., Fidler, S., Barriuso, A., Torralba, A.: Semantic understanding of scenes through the ade20k dataset. International Journal of Computer Vision **127**(3), 302–321 (2019)